European Journal of Radiology 115 (2019) 22–30

Contents lists available at ScienceDirect

European Journal of Radiology

journal homepage: www.elsevier.com/locate/ejrad

Research article

Solitary pulmonary nodule: Comparison of quantitative capability for differentiation and management among dynamic CE-perfusion MRI at 3 T system, dynamic CE-perfusion ADCT and FDG-PET/CT

Yoshiharu Ohno[a,b,c,*], Yasuko Fujisawa[d], Masao Yui[d], Daisuke Takenaka[e], Hisanobu Koyama[f], Naoki Sugihara[d], Takeshi Yoshikawa[a,b]

[a] Division of Functional and Diagnostic Imaging Research, Department of Radiology, Kobe University Graduate School of Medicine, Kobe, Japan
[b] Advanced Biomedical Imaging Research Center, Kobe University Graduate School of Medicine, Kobe, Japan
[c] Department of Radiology, Fujita Health University School of Medicine
[d] Canon Medical Systems Corporation, Otawara, Japan
[e] Department of Radiology, Hyogo Cancer Center, Akashi, Japan
[f] Department of Radiology, Osaka Police Hospital, Osaka, Japan

ARTICLE INFO

Keywords:
Lung
Nodule
CT
MRI
PET/CT
Perfusion

ABSTRACT

Purpose: To prospectively compare the capability of dynamic first-pass contrast-enhanced (CE) perfusion MR imaging with ultra-short TE and area-detector CT (ADCT), analyzed with the same mathematical methods, and that of FDG-PET/CT for diagnosis and management of solitary pulmonary nodules (SPNs).

Methods and materials: Our institutional review board approved this study and written informed consent was obtained from all subjects. A total 57 consecutive patients with 71 nodules prospectively underwent dynamic CE-perfusion ADCT and MR imaging with ultra-short TE, FDG-PET/CT, as well as microbacterial and/or pathological examinations. The nodules were classified into malignant nodules (n = 45) and benign nodules (n = 26). Pulmonary arterial, systemic arterial and total perfusions were determined by means of dual-input maximum slope models on ADCT and MR imaging and maximum values of standard uptake values (SUV_{max}) on PET/CT. Receiver operating characteristic (ROC) analysis was performed for each index, and sensitivity, specificity and accuracy were compared by McNemar's test.

Results: Areas under the curve (Azs) of total perfusion on ADCT (Az = 0.89) and MR imaging (Az = 0.88) were significantly larger than those of systemic arterial perfusion and MR imaging ($p < 0.05$). Accuracy of total perfusion on ADCT (87.3% [62/71]) and MR imaging (87.3% [62/71]) was significantly higher than that of systemic arterial perfusion for both methods (77.5% [55/71] $p = 0.02$) and SUV_{max} (78.9% [56/71], $p = 0.03$).

Conclusion: Dynamic CE-perfusion MR imaging with ultra-short TE and ADCT and have similar potential capabilities, and are superior to FDG-PET/CT in this setting.

1. Introduction

Pulmonary nodules are common findings on chest radiography and computed tomography (CT) images, and clinicians are frequently asked to differentiate malignant from benign nodules for management in the least invasive manner. Dynamic contrast-enhanced (CE-) single-detector or multi-detector row CTs, dynamic CE-magnetic resonance (MR) imaging and positron emission tomography (PET) or PET combined with CT (PET/CT) using 2-[fluorine-18]-fluoro-2-deoxy-D-glucose (FDG) have been evaluated or adopted for diagnosis and/or management of solitary pulmonary nodules (SPNs) in routine clinical practice [1–16]. A meta-analysis study published in 2008 suggested that none of these modalities is significantly better than the others for diagnosis of patients with SPNs [8]. On the other hand, a direct comparative study demonstrated that semi-quantitative assessment of first-pass components of dynamic first-pass CE-MR imaging with ultra-short TE could diagnose SPNs with higher specificity and/or accuracy than dynamic CE-MDCT or integrated PET/CT [3,9].

Since 2011, a 320-detector row CT system with an area detector (known as an area detector CT or ADCT) has been used for dynamic

* Corresponding author at: Division of Functional and Diagnostic Imaging Research, Department of Radiology, Kobe University Graduate School of Medicine, 7-5-2 Kusunoki-cho, Chuo-ku, Kobe, Hyogo, 650-0017, Japan. Tel.: +81-78-382-6104; fax: +81-78-382-6129
E-mail addresses: yosirad@kobe-u.ac.jp, yosirad@med.kobe-u.ac.jp, yohno@fujita-hu.ac.jp (Y. Ohno).

https://doi.org/10.1016/j.ejrad.2019.03.018
Received 3 January 2019; Received in revised form 20 February 2019; Accepted 24 March 2019

first-pass CE-perfusion ADCT and has been tested for not only diagnosis, but also management of SPNs and non-small cell lung cancer [12–18]. In addition, quantitatively assessed dynamic first-pass CE-perfusion ADCT with dual-input maximum slope model was recommended in 2015 as being able to differentiate malignant from benign nodules more specifically and accurately than semi-quantitatively assessed dynamic first-pass CE-perfusion MR imaging with ultra-short TE and quantitatively analyzed FDG-PET/CT [17]. Therefore, the first-pass component of a dynamic perfusion study has better potential for more specific and/or accurate differentiation than glucose metabolism in routine clinical practice. Moreover, it has been suggested that the application of an appropriate mathematical model is one of the key issues for an effective diagnosis based on quantitatively assessed dynamic first-pass CE-perfusion ADCT [13–18]. In addition, dynamic CE-MR imaging using the first-pass perfusion technique is also considered as useful in this setting, when applied same mathematical model. To the best of our knowledge, however, no studies have been reported that directly compared the diagnostic performance of dynamic first-pass CE-perfusion ADCT and MR imaging, analyzed with the same mathematical model, with that of FDG-PET/CT for differentiating malignant from benign SPNs and distinguishing between SPNs requiring further evaluation of SPNs and those needing only follow-up examination.

We hypothesized that dynamic first-pass CE-perfusion MR imaging with ultra-short echo-time (TE) and ADCT, using the same mathematical model, have better potential capability than FDG-PET/CT for differentiation of malignant from benign SPNs and management of SPNs. The purpose of our study was therefore to prospectively compare the capability for diagnosis and management of SPNs of dynamic first-pass CE-perfusion MR imaging with ultra-short TE and ADCT, analyzed with the same mathematical methods with that of FDG-PET/CT.

2. Materials and methods

2.1. Subjects

This prospective study was approved by our institutional review board of Kobe Unjversity Hospital and written informed consent was obtained from each subject. It was financially and technically supported by Canon Medical Systems Corporation, and financially by Grants-in-Aid for Scientific Research from the Japanese Ministry of Education, Culture, Sports, Science and Technology and the Adaptive and Seamless Technology Transfer Program through Target Driven R & D from the Japan Science and Technology. Three of the authors (Y.F, M.Y, N.S) are employees of Canon Medical Systems but did not have control over any of the data and information submitted for publication or which data and information were to be included in this study. All data in this study were managed by other radiologists.

Sixty-nine consecutive patients (45 men and 24 women, mean age, 68.0 years; age range, 36–85 years) were referred to our hospital with suspected SPNs, identified on chest radiographs or CT performed at our hospital or local hospitals or clinics. The patients who were selected for this study met the following criteria: (a) presence of pulmonary nodules more than 8 mm and less than 30 mm in greatest diameter on all three planes and without calcification, (b) no contraindications for the administration of iodinated and gadolinium contrast media, and (c) ability to participate cooperatively in the procedures. Diameter was defined as the greatest diameter observed on conventional thin-section ADCT scans obtained with a lung window setting. No calcification in pulmonary nodules was defined as absence of visible calcification on conventional thin-section ADCT scans (1-mm section thickness) obtained with a mediastinal window setting. A total of twelve patients were subsequently excluded, six because no pulmonary nodules were detected, three due to contraindications for iodinated and/or gadolinium contrast medium administration, two after calcification was detected within the nodules, and one due to non-cooperation with the procedures.

The study group thus comprised 57 consecutive patients, 38 males (mean age ± SD: 69.7 ± 5.8 years) and 19 females (mean age ± SD: 69.7 ± 6.4 years). These patients with 71 pulmonary nodules (mean diameter ± SD: 17.5 ± 4.5; diameter range: 9–29 mm) prospectively underwent several of the following procedures: dynamic first-pass CE-perfusion ADCT, dynamic first-pass CE-MR imaging with ultra-short TE, integrated PET/CT with FDG, transbronchial or percutaneous biopsies, bronchoalveolar lavage, microbiological examinations, resection by thoracotomy and video-assisted thoracic surgery (VATS) and follow-up CT examinations. Based on CT findings, 71 nodules were divided as three nodule types as follows: 43 solid nodules, 21 part solid nodules and 7 ground glass nodules.

Every patient underwent all radiological examinations within two weeks (mean: 4.9 days; range: 1–12 days). All biopsies and/or bronchoalveolar lavages were performed within one week (mean: 3.2 days; range: 1–12 days) after all radiological examinations. All subsequent surgical treatments were performed within three weeks (mean: 15.7 days; range: 13–28 days) after pathological and/or microbiological examination of specimens obtained by means of biopsy and/or bronchoalveolar lavage. Final diagnoses for all patients were confirmed by microbiological examination ($n = 26$), cytological or histological examination of specimens obtained by CT-guided transthoracic needle biopsy ($n = 6$), transbronchial lung biopsy ($n = 24$) or surgical resection ($n = 23$) and follow-up CT examinations ($n = 18$). Follow-up CT examinations were performed every six months for more than two years after the initial dynamic first-pass perfusion ADCT and PET/CT examinations.

Nodules were classified into three groups based on the final diagnosis. One group comprised malignant nodules ($n = 45$), which were subdivided into 43 primary peripheral lung cancers (twenty-four invasive adenocarcinomas, eight adenocarcinomas in situ, five squamous cell carcinomas, three minimally invasive adenocarcinomas, two adenosquamous cell carcinomas, and one small cell carcinoma) and two metastatic lung tumors originating from one colon cancer and one laryngeal cancer. The other two groups comprised benign nodules with low biological activity ($n = 18$, comprising fifteen organizing pneumonias, whose size remained unchanged for more than two years, two tuberculomas and one hamartoma) and benign nodules with high biological activity ($n = 8$, comprising four organizing pneumonias with reduced size after treatment or during follow-up examination, two atypical mycobacterium infections, one cryptococcosis and one pulmonary tuberculosis). Based on the results of pathological, mycrobacterial and/or follow-up examinations, all benign nodules with low biological activities were defined as nodules requiring follow-up examination, but no further intervention or treatment. All tuberculomas, hamartomas, atypical mycobacterial infections, and cases of cryptococcosis and pulmonary tuberculosis were confirmed by histological examinations from specimens obtained by surgical resection, CT-guided or transbronchial biopsies and/or follow-up CT examinations after treatment. In addition, all organizing pneumonias were also confirmed by pathological and microbiological examinations as well as follow-up CT examinations. The following criteria were used to distinguish tuberculomas from active tuberculosis: (a) no evidence of change in size at follow-up CT examinations every six months for more than two years and (b) no evidence of the presence of *Mycobacterium tuberculosis* during mycobacterial examination.

Of the fifty-seven patients, seven had two, two had three and one had four pulmonary nodules. Of these twenty-four pulmonary nodules, fifteen were detected within the same scan range, and nine within different scan ranges, even though whole-lung dynamic first-pass CE-perfusion ADCT examination with two or three wide scan volumes for the same examinations.

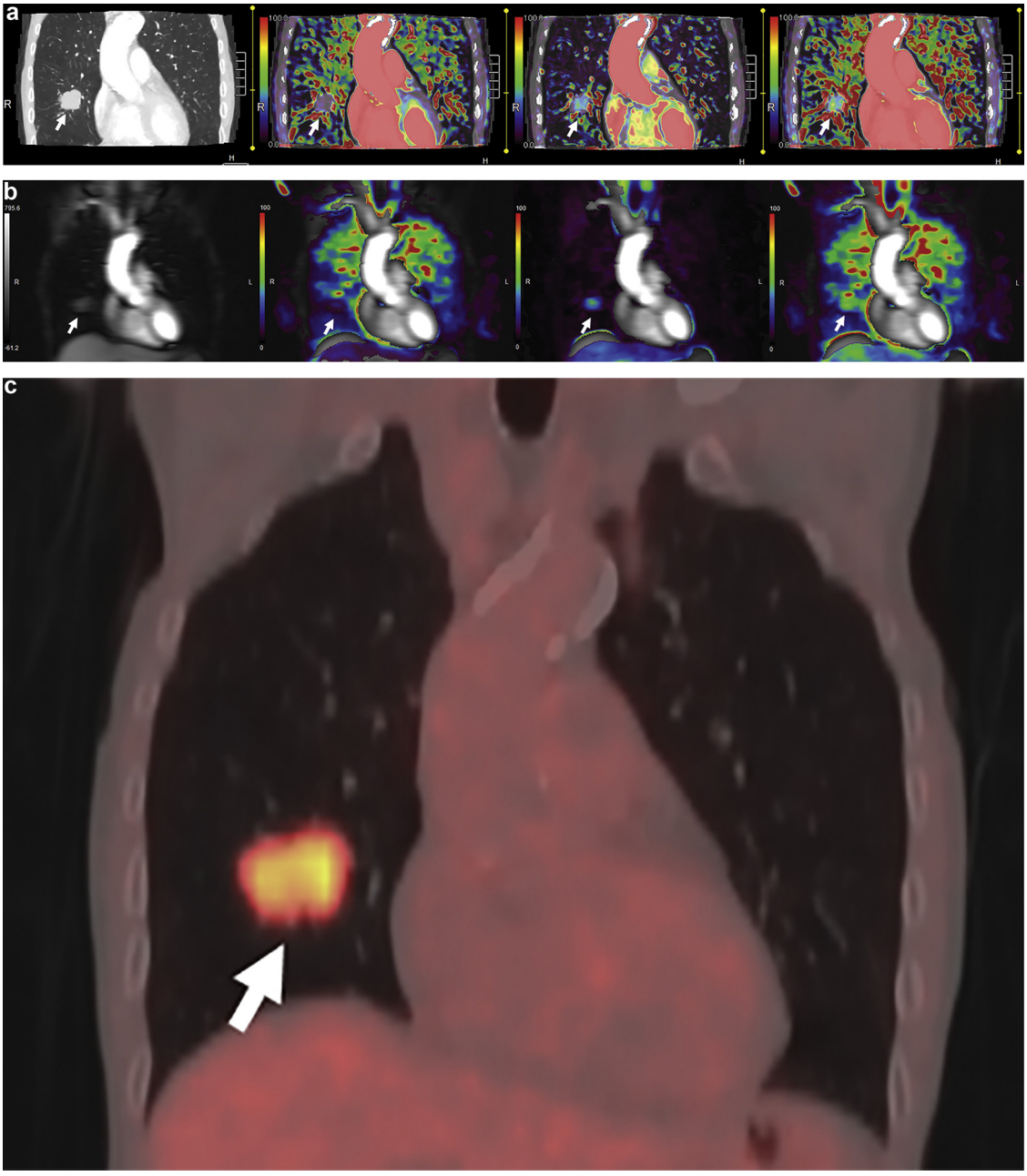

Fig. 1. 80-Year-old female patient with adenocarcinoma with lepidemic pattern. (A) (L to R: thin-section multiplanar reformatted (MPR) image from thin-section CT data and from pulmonary arterial perfusion, systemic arterial perfusion and total perfusion maps). Thin-section MPR image shows a nodule (arrow) with a diameter of 21 mm in the right middle lobe. Dynamic first-pass CE-perfusion ADCT assessed with the dual-input maximum slope method provided perfusion maps which also show a nodule (arrow). Pulmonary arterial perfusion, systemic arterial perfusion and total perfusion were 13.0 ml/100 ml/min, 25.9 ml/100 ml/min and 39.0 ml/100 ml/min, respectively. The three feasible threshold values led to an assessment of this nodule as malignant or as requiring further intervention and treatment. This case was true-positive for all perfusion indices. (B) (L to R: source image, pulmonary arterial perfusion, systemic arterial perfusion and total perfusion maps). Dynamic first-pass CE-perfusion MR imaging with ultra-short TE assessed with the dual-input maximum slope method produces perfusion maps, which also show a nodule (arrow). Pulmonary arterial perfusion, systemic arterial perfusion and total perfusion were 11.0 ml/100 ml/min, 31.4 ml/100 ml/min and 42.5 ml/100 ml/min, respectively. The three feasible threshold values led to an assessment of this nodule as malignant or as requiring further intervention and treatment. This case was true-positive case for all perfusion indices. (C) PET/CT shows a nodule (arrow) with high uptake of FDG and SUV_{max} evaluated as 4.0. According to the feasible threshold value, this nodule was assessed as malignant or as requiring further intervention and treatment. This case was true-positive case on SUV_{max}.

2.2. Dynamic first-pass CE-MR imaging with ultra-short TE on a 3 T MR system

All MR studies were performed with a 3 T superconducting magnet (Vantage Titan 3 T; Canon Medical Systems, Otawara, Japan) using a phased array coil (SPEEDER coil; Canon Medical Systems) with parallel imaging capability. Dynamic MR images (TR 3.0 ms/TE 1.1 ms/flip angle 12°, reduction factor 2, 256 × 64 matrix, 512 × 128 reconstructed matrix, field of view; 500 × 350 mm) were acquired with a three-dimensional (3D) fast field echo sequence without fat suppression pulse. All dynamic MR studies were performed with the patient's arms placed above the head for reduction of partial phase FOV. A 3D-slab with a thickness of 135 mm including entire lung was used with 36 partitions in the coronal plane in a left-to-right phase-encoded direction, resulting in an effective partition thickness of 3.75 mm and real-phase encoding in the slice direction of 14 steps with partial Fourier

Table 1
Parameters for the malignant and benign nodule groups with predicted high and low biological activities.

	Index	Malignant nodules (n = 45)	Benign nodules with predicted high biological activity (n = 8)		Benign nodules with predicted low biological activity (n = 18)		
		(Mean ± SD)	(Mean ± SD)	p Value (vs. malignant)	(Mean ± SD)	p Value (vs. malignant)	p Value (vs. high biological)
Dynamic first-pass CE-perfusion ADCT	Longest diameter (mm)	17.8 ± 4.1	17.0 ± 6.2	0.89	16.7 ± 5.0	0.67	0.99
	Smoking history (pack-year)	42.8 ± 32.0	42.1 ± 40.8	0.99	49.7 ± 42.0	0.77	0.87
	Total perfusion (ml/100 ml/min)	60.8 ± 34/8	37.5 ± 28.9	0.11	14.0 ± 8.4*	< 0.0001	0.16
	Pulmonary arterial perfusion (ml/100 ml/min)	28.4 ± 23.8	15.7 ± 12.9	0.23	10.2 ± 6.8*	0.004	0.79
	Systemic arterial perfusion (ml/100 ml/min)	32.4 ± 24.0	21.8 ± 18.5	0.37	3.9 ± 3.2*	< 0.0001	0.10
Dynamic first-pass CE-perfusion MR imaging with ultra-short TE	Total perfusion (ml/100 ml/min)	70.9 ± 41.0	43.3 ± 33.2	0.11	17.3 ± 10.4*	< 0.0001	0.19
	Pulmonary arterial perfusion (ml/100 ml/min)	36.9 ± 30.9	20.4 ± 16.8	0.23	13.2 ± 8.8*	0.004	0.79
	Systemic arterial perfusion (ml/100 ml/min)	34.0 ± 25.2	22.9 ± 19.4	0.37	4.1 ± 3.3*	< 0.0001	0.10
FDG-PET/CT	SUV_{max}	3.7 ± 1.6	3.1 ± 1.6	0.43	2.0 ± 0.5*	< 0.0001	0.17

SD: standard deviation.
* Significant difference from malignant nodule group (p < 0.05).

Fig. 2. ROC analyses of three radiological indices used for differentiating malignant from benign nodules (red line: total perfusion on dynamic first-pass CE-perfusion ADCT, blue line: pulmonary arterial perfusion on dynamic first-pass CE-perfusion ADCT, green line: systemic arterial perfusion on dynamic first-pass CE-perfusion ADCT, pink line: total perfusion on dynamic first-pass CE-perfusion MR imaging, sky blue line: pulmonary arterial perfusion on dynamic first-pass CE-perfusion MR imaging, yellow-green line: systemic arterial perfusion on dynamic first-pass CE-perfusion MR imaging, yellow line: SUV_{max}). Areas under the curve (Azs) of the indices on dynamic first-pass CE-perfusion ADCT were: total perfusion, Az = 0.89; pulmonary arterial perfusion, Az = 0.81; systemic arterial perfusion, Az = 0.75. On dynamic first-pass CE-perfusion MR imaging with ultra-short TE, they were: total perfusion, Az = 0.88; pulmonary arterial perfusion, Az = 0.81; systemic arterial perfusion, Az = 0.75. Az of SUV_{max} was determined as 0.80. Azs of total perfusion determined with the two methods were significantly larger than those of systemic arterial perfusion determined with ADCT (p < 0.05) and MR imaging with ultra-short TE (p < 0.05). The feasible threshold values of all indices on dynamic first-pass CE-perfusion ADCT were determined as 29.0 ml/100 ml/min for total perfusion, 10.0 ml/100 ml/min for pulmonary arterial perfusion, and 11.2 ml/100 ml/min for systemic arterial perfusion. The corresponding feasible threshold values on dynamic first-pass CE-perfusion MR imaging with ultra-short TE were: 36.0 ml/100 ml/min, 10.5 ml/100 ml/min, 14.0 ml/100 ml/min. The feasible threshold value on SUV_{max} was determined as 2.5.

reconstruction. This means that the spatial resolution of dynamic first-pass CE-MR imaging was 7.81 mm (x-axis) × 1.36 mm (y-axis) × 7.5 mm (z-axis), and the temporal resolution was 1.565 s (3 ms × 64 step × 14 step × 1/2 < reduction factor > with 21 ms fat suppression pre-pulse and 200 ms waiting time) for each 3D data set. Gadolinium contrast medium (0.1 ml/kg) (Magnescope, gadoterate meglumine [Gd-DOTA]; Guerbet Japan, Tokyo, Japan) was bolus administered to all patients via a cubital vein with an automatic infusion system (Sonic shot, Nemoto) at a rate of 5 mL/s, followed by 20 mL of saline solution at the same rate. The dynamic first-pass CE-MR sequence was initiated at the time of the contrast medium injection. Before the MR studies, patients were carefully instructed in the breath-holding technique and practiced it to reproduce exactly the same degree of inspiration for each scan series. With each scan, 20 images were obtained during 32 s of breath holding at end-inspiration. All 53 dynamic first-pass CE-MR examinations were completed successfully without any adverse effects.

2.3. Dynamic first-pass CE-ADCT and integrated FDG-PET/CT examination

All dynamic first-pass CE-ADCT studies were performed on a 320-detector row CT scanner (Aquilion ONE; Canon Medical) using

Table 2
Feasible threshold values, sensitivity, specificity, positive predictive values, negative predictive values and accuracy of three perfusion parameters from dynamic first-pass perfusion CE-ADCT and MR imaging with ultra-short TE and of SUV_{max} on PET/CT for differentiation of malignant from benign nodules.

	Index	Threshold value		SE	SP	PPV	NPV	AC
Dynamic first-pass CE-perfusion ADCT	Total perfusion (ml/100 ml/min)	29.0	%	91.1	80.8	89.1	84.0	87.3
			Cases	(41/45)	(21/26)	(41/46)	(21/25)	(62/71)
	Pulmonary arterial Perfusion (ml/100 ml/min)	10.0	%	84.4	76.9	86.4	74.1	81.7
			Cases	(38/45)	(20/26)	(38/44)	(20/27)	(58/71)
	Systemic arterial perfusion (ml/100 ml/min)	11.2	%	84.4	65.4	80.9	70.8	77.5*,**
			Cases	(38/45)	(17/26)	(38/47)	(17/24)	(55/71)
Dynamic first-pass CE-perfusion MR imaging with ultra-short TE	Total perfusion (ml/100 ml/min)	36.0	%	88.9	84.6	90.9	81.5	87.3
			Cases	(40/45)	(22/26)	(40/44)	(22/27)	(62/71)
	Pulmonary arterial perfusion (ml/100 ml/min)	10.5	%	84.4	76.9	86.4	74.1	81.7
			Cases	(38/45)	(20/26)	(38/44)	(20/27)	(58/71)
	Systemic arterial perfusion (ml/100 ml/min)	14.0	%	84.4	65.4	80.9	70.8	77.5*,**
			Cases	(38/45)	(17/26)	(38/47)	(17/24)	(55/71)
FDG-PET/CT	SUV_{max}	2.5	%	82.2	73.1	84.1	70.4	78.9*,**
			Cases	(37/45)	(19/26)	(37/44)	(19/27)	(56/71)

SE: sensitivity, SP: specificity, PPV: positive predictive value, NPV: negative predictive value, AC: accuracy, 95% CI: 95% confidence interval.
* Significant difference from total perfusion on dynamic first-pass CE-perfusion ADCT ($p < 0.05$).
** Significant difference from total perfusion on dynamic first-pass CE-perfusion MR imaging with ultra-short TE ($p < 0.05$).

volumetric cine scan without helical scan at two or three different positions to cover the entire lung [12–18]. Dynamic ADCT examination was performed at intervals of at least 5 min between each volume position. Details of dynamic first-pass CE-perfusion ADCT examination are described in the literatures [12–18]. The estimated volume computed tomography dose index (CTDIvol [e.g., and the following parameters]) displayed on the CT scanner console was recorded for each patient. These values were based on the weighted computed tomography dose index (CTDIw [e.g., tube voltage or tube current]). CTDIvol obtained with each of the dynamic first-pass perfusion ADCT studies was 16.0 mGy. The estimated dose length product (DLP) was calculated as CTDIvol × scan length, which was determined as 343.3–514.9 mGy × cm, with the effective dose for this protocol estimated at 4.81–7.21 mSv [12–18].

For integrated FDG-PET/CT examination, each patient fasted for at least 6 h before the intravenous administration of FDG at a rate of 3.3 MBq/kg BW, and images were obtained from the skull to the mid-thigh 60 min after completion of the injection. All FDG-PET/CT examinations were performed with a commercially available PET/CT scanner (Discovery ST; GE Health Care, Milwaukee, WI) and a standard lung cancer staging protocol described in the past literatures [12,14,15,17].

2.4. Image analysis

All dynamic first-pass CE-perfusion ADCT and dynamic first-pass CE-perfusion MR imaging data were also transferred to a personal computer (Precision; DELL, Kawasaki, Kanagawa, Japan), and automated 3D motion corrections were performed with software, the details of which were published in a technical manuscript [19]. In addition, dynamic ADCT data obtained at each position were combined to generate dynamic first-pass CE- whole-lung perfusion ADCT images by means of commercially available software provided by Canon Medical. In this study, our proprietary CT software (Advanced Body Perfusion; Canon Medical Systems) and proprietary MR software (Canon Medical) were used for all analyses. All quantitatively analyzed ADCT and MR indices were analyzed on a pixel-by-pixel basis. Then, regions of interest (ROIs; diameter range: 8–29 mm) were placed by two board certified chest radiologists with 24 years' experience (Y.O) and 13 years' experience (H.K) over each targeted lesion, the main trunk of the pulmonary artery, the lung parenchyma and/or descending aorta. An ROI was placed over each nodule, encompassing its entire cross-sectional area, and made as large as possible to minimize the effects of tumoral hemodynamic inhomogeneities. For perfusion parameter measurements, ROIs were placed over all slices of a given nodule, and the indices determined for each slice were also averaged. Density-time or signal intensity–time curves of a nodule were generated for a mediastinal window setting or un-enhanced FFE image that ensured that the need for partial volume averaging was minimized. For this study, quantitatively analyzed ADCT and MR indices were calculated by using the dual-input maximum slope method selected on the basis past study results [13–18]. In this study, total, pulmonary arterial and systemic arterial perfusions within a lesion were calculated with the formulas described in the past literatures and expressed in ml/100 ml/min [13–18]. For dynamic first-pass CE-perfusion ADCT and MR imaging with ultra-short TE, all dynamic CE-perfusion indices were measured twice, and the final value was determined as the average of the first and second measurements.

For FDG-PET/CT images, SUV data were overlaid on conventional plain MDCT with the lung window set for an FDG-PET/CT section thickness of 5 mm. ROIs (diameter range 8–29 mm) were then placed over each nodule for determination of the maximum value of SUV (SUV_{max}) by two general radiologists with 23 years' (T.Y) and 28 years' (D.T) overall experience and more than 10 years' experience as PET physicians. To minimize the effects of metabolic inhomogeneities within each targeted lesion, the ROI was made as large as possible and placed over each of the targeted lesions so as to encompass the entire cross-sectional area of the lesion. ROIs were placed over each of the targeted lesions in all of the slices, and the SUV_{max} values for the slices were also averaged to obtain the mean SUV_{max} value for every measurements. SUV_{max} was measured twice and averaged to obtain the final value for each lesion as determined by either investigator.

2.5. Statistical analysis

2.5.1. Intra- and inter-observer agreements

For intra-observer agreement evaluation for two investigators, the Bland–Altman analysis was used to compare the reproducibility coefficients of all perfusion parameters on dynamic first-pass CE-perfusion ADCT and MR imaging with ultra-short TE and SUV_{max} [20], while correlation between first and second measurements of each of the indices was also assessed by Pearson's correlation.

For assessment of inter-observer agreement for every index, correlations between individual index measurements made by each of the two investigators and then averaged, were statistically determined by Pearson's correlation. In addition, inter-observer agreement for every index was determined as the limit of agreement determined with the Bland–Altman analysis [20].

Table 3
Parameters of nodules requiring aggressive intervention and treatment and those needing only follow-up examination.

		Nodules requiring aggressive intervention and treatment (n = 53) (Mean ± SD)	Nodules needing only follow-up examination (n = 18) (Mean ± SD)	p Value
	Longest diameter (mm)	17.7 ± 4.4	16.7 ± 5.0	0.16
	Smoking history (pack-year)	42.7 ± 33.3	49.7 ± 42.0	0.47
Dynamic first-pass CE-perfusion ADCT	Total perfusion (ml/100 ml/min)	57.3 ± 34.7	14.0 ± 8.4*	< 0.0001
	Pulmonary arterial perfusion (ml/100 ml/min)	30.8 ± 23.4	3.9 ± 3.2*	< 0.0001
	Systemic arterial perfusion (ml/100 ml/min)	26.5 ± 22.9	10.2 ± 6.8*	0.002
Dynamic first-pass CE-perfusion MR imaging with ultra-short TE	Total perfusion (ml/100 ml/min)	66.8 ± 40.9	17.3 ± 10.4*	< 0.0001
	Pulmonary arterial perfusion (ml/100 ml/min)	32.3 ± 24.6	4.1 ± 3.3*	< 0.0001
	Systemic arterial perfusion (ml/100 ml/min)	34.5 ± 29.7	13.2 ± 8.8*	0.002
FDG-PET/CT	SUV_{max}	3.6 ± 1.6	2.0 ± 0.5*	< 0.0001

SD: standard deviation.
* Significant difference from nodules requiring further intervention and treatment ($p < 0.05$).

Fig. 3. ROC analyses of three radiological indices used for differentiating nodules requiring aggressive intervention and treatment from nodules needing only follow-up examination (for clarification of the seven lines, refer to the legend for Fig. 2). Areas under the curve (Azs) of the indices on dynamic first-pass CE-perfusion ADCT were: total perfusion, Az = 0.94; pulmonary arterial perfusion, Az = 0.89; systemic arterial perfusion, Az = 0.77. On dynamic first-pass CE-perfusion MR imaging with ultra-short TE, they were: total perfusion, Az = 0.92; pulmonary arterial perfusion, Az = 0.89; systemic arterial perfusion, Az = 0.77. Az of SUVmax was determined as 0.85. Azs of total perfusion determined with the two methods were significantly larger than those of systemic arterial perfusion determined with ADCT ($p < 0.05$) and MR imaging with ultra-short TE ($p < 0.05$). The feasible threshold values of all indices on dynamic first-pass CE-perfusion ADCT were determined as: total perfusion: 28.5 ml/100 ml/min for total perfusion, 9.0 ml/100 ml/min for pulmonary arterial perfusion, and 11.0 ml/100 ml/min for systemic arterial perfusion. The corresponding feasible threshold values on dynamic first-pass CE-perfusion MR imaging with ultra-short TE were: 35.0 ml/100 ml/min, 10.0 ml/100 ml/min, and 14.5 ml/100 ml/min. The feasible threshold value on SUV_{max} was determined as 2.5.

2.5.2. Inter-method agreement between assessments for each perfusion parameter made by dynamic first-pass CE-perfusion ADCT and MR imaging with ultra-short TE

To determine inter-method agreements for the indices, correlation between dynamic first-pass CE-perfusion ADCT and MR imaging with ultra-short TE was statistically assessed by means of Person's correlation. In addition, the limits of agreement between two methods for each index was also assessed with the Bland–Altman analysis [20].

2.5.3. Malignant nodules vs. benign nodules with predicted high biological activity vs. benign nodules with predicted low biological activity

To determine differences among malignant nodules, benign nodules with predicted high and with predicted low biological activity, the largest diameter, smoking history, all perfusion parameters on dynamic first-pass CE-perfusion ADCT and MR imaging with ultra-short TE and the SUV_{max} of the three groups were compared with the aid of analysis of variance using Tukey's honestly significant difference test.

Receiver operating characteristics (ROC) analyses were performed to determine feasible threshold values for each index used for differentiating malignant from benign nodule groups. Finally, the McNemar test was used to compare the sensitivity, specificity and accuracy of dynamic first-pass CE-perfusion ADCT and dynamic first-pass CE-MR indices and SUV_{max} for distinguishing malignant from benign pulmonary nodules.

Table 4
Feasible threshold values, sensitivity, specificity, positive predictive values, negative predictive values and accuracy of perfusion parameters on dynamic first-pass perfusion CE-ADCT and MR imaging with ultra-short TE and of SUV_{max} from PET/CT for differentiation of nodules requiring aggressive intervention and treatment from those needing only follow-up examination.

	Index	Threshold value		SE	SP	PPV	NPV	AC
Dynamic first-pass CE-perfusion ADCT	Total perfusion (ml/100 ml/min)	28.5	%	86.8	100.0	100.0	72.0	90.1
			Cases	(46/53)	(18/18)	(46/46)	(18/25)	(64/71)
	Pulmonary arterial perfusion (ml/100 ml/min)	9.0	%	83.0	94.4	97.8	65.4	85.9
			Cases	(44/53)	(17/18)	(44/45)	(17/26)	(61/71)
	Systemic arterial perfusion (ml/100 ml/min)	11.0	%	81.1	77.8	91.5	58.3	80.3*,**
			Cases	(43/53)	(14/18)	(43/47)	(14/24)	(57/71)
Dynamic first-pass CE-perfusion MR imaging with ultra-short TE	Total perfusion (ml/100 ml/min)	35.0	%	84.9	100.0	100.0	69.2	88.7
			Cases	(45/53)	(18/18)	(45/45)	(18/26)	(63/71)
	Pulmonary arterial perfusion (ml/100 ml/min)	10.0	%	83.0	94.4	97.8	65.4	85.9
			Cases	(44/53)	(17/18)	(44/45)	(17/26)	(61/71)
	Systemic arterial perfusion (ml/100 ml/min)	14.5	%	81.1	77.8	91.5	58.3	80.3*,**
			Cases	(43/53)	(14/18)	(43/47)	(14/24)	(57/71)
FDG-PET/CT	SUV_{max}	2.5	%	77.4	83.3	93.2	55.6	78.9*,**
			Cases	(41/53)	(15/18)	(41/44)	(15/27)	(56/71)

SE: sensitivity, SP: specificity, PPV: positive predictive value, NPV: negative predictive value, AC: accuracy, 95% CI: 95% confidence interval.
* Significant difference from total perfusion on dynamic first-pass CE-perfusion ADCT ($p < 0.05$).
** Significant difference from total perfusion on dynamic first-pass CE-perfusion MR imaging with ultra-short TE ($p < 0.05$).

2.5.4. Nodules requiring aggressive intervention and treatment vs. nodules needing only follow-up examination

To identify the differences between nodules requiring aggressive intervention and treatment (i.e. biopsy and/or treatment including resection), which consisted of malignant and benign nodules with predicted high biological activity, and nodules needing only follow-up examination, which consisted of benign nodules with predicted low biological activity, the largest diameter, smoking history, all perfusion parameters on dynamic first-pass CE-perfusion ADCT and MR imaging with ultra-short TE and SUV_{max} of the two groups were compared by means of the unequal variance *t*-test.

This was followed by ROC analyses to determine feasible threshold values and compare the diagnostic capability of dynamic first-pass CE-perfusion ADCT, dynamic first-pass CE-MR imaging with ultra-short TE and PET/CT indices for identification of significant differences between nodules requiring aggressive intervention and treatment and those needing only follow-up examination. The McNemar test was then used to compare the sensitivity, specificity and accuracy of dynamic first-pass perfusion ADCT indices and SUV_{max} for distinguishing the two types of nodules.

All statistical analyses were evaluated with commercially available statistical software (JMP 11; SAS Institute Japan, Tokyo, Japan). *P* values < 0.05 were considered statistically significant.

3. Results

Representative cases are shown in Fig. 1. No adverse effects from the procedures used for this study were observed in these cases.

3.1. Intra- and inter-observer agreement assessments

Correlations between the first and second measurements of each index ranged from significant to excellent ($r = 0.99$, $p < 0.0001$). Mean differences in each index between first and second measurements ranged from −0.1 ml/100 ml/min to 0.1 ml/100 ml/min. Reproducibility coefficients for all indices between first and second measurements ranged from 0.4 ml/100 ml/min to 3.6 ml/100 ml/min, and were small enough for clinical purposes.

Inter-observer agreements for assessments of all indices, correlation and the limits of agreement by the two investigators are shown in supplement material Table E1. Correlations between the first and second measurements of all indices ranged from significant to excellent ($r = 0.99$, $p < 0.0001$). In addition, the limits of agreements for total perfusion, pulmonary arterial perfusion, systemic arterial perfusion and SUV_{max} were small enough for clinical purposes.

3.2. Inter-method agreement between dynamic first-pass CE-perfusion ADCT and MR imaging with ultra-short TE for assessment of perfusion parameters

Results of correlation analysis and the limits of agreement for each index between the two methods are shown in supplement material Table E2. There was significant and excellent correlation for each perfusion index ($r = 0.99$, $p < 0.0001$), and the limits of agreement between the two methods were also determined as small enough for clinical purpose.

3.3. Malignant nodules vs. benign nodules

Long-axis diameter, all perfusion parameters and SUV_{max} for malignant and benign nodules with predicted high and low activities are shown in Table 1. Total and systemic arterial perfusions evaluated by dynamic first-pass CE-perfusion ADCT and MR imaging with ultra-short TE and SUV_{max} of the malignant nodule group were significantly higher than those of the benign nodules with predicted low biological activity ($p < 0.0001$). In addition, pulmonary arterial perfusions evaluated by the two methods of the malignant nodules were significantly higher than those of the benign nodules with predicted low biological activity ($p = 0.004$).

The results of ROC analysis for differentiating malignant from benign nodules are shown in Fig. 2. Areas under the curve (Azs) of total perfusion assessed by dynamic first-pass CE-perfusion ADCT (Az = 0.89) and MR imaging with ultra-short TE (Az = 0.88) were significantly larger than those of systemic arterial perfusion assessed by dynamic first-pass CE-perfusion ADCT (Az = 0.75, $p < 0.05$) and MR imaging with ultra-short TE (Az = 0.75, $p < 0.05$).

The diagnostic capability of the radiological indices for differentiating between malignant and benign nodules is shown in Table 2. When applied each feasible threshold value, accuracy of total perfusion on dynamic first-pass CE-perfusion ADCT (87.3% [62/71]) and MR imaging with ultra-short TE (87.3% [62/71]) was significantly higher than that of systemic arterial perfusion using the two methods (77.5% [55/71], $p = 0.02$) and SUV_{max} (78.9% [56/71], $p = 0.03$).

3.4. Nodules requiring aggressive intervention and treatment vs. nodules needing only follow-up examination

Long-axis diameter, dynamic first-pass CE- perfusion ADCT indices,

dynamic first-pass CE-MR indices and SUV_{max} for nodules requiring aggressive intervention and treatment and those needing only follow-up examination are shown in Table 3. Total and pulmonary arterial perfusions evaluated by dynamic first-pass CE-perfusion ADCT and MR imaging with ultra-short TE and SUV_{max} of the malignant nodule group were significantly higher than those of benign nodules with predicted low biological activity ($p < 0.0001$). In addition, systemic arterial perfusions evaluated in the same manner were significantly higher for the malignant than for the benign nodules with predicted low biological activity ($p = 0.002$).

The results of ROC analyses of radiological indices which showed significant differences between nodules requiring aggressive intervention and treatment and those needing only follow-up examination are shown in Fig. 3. Areas under the curves (Azs) of total perfusion assessed by dynamic first-pass CE-perfusion ADCT (Az = 0.94) and MR imaging with ultra-short TE (Az = 0.92) were significantly larger than those of systemic arterial perfusion assessed by dynamic first-pass CE-perfusion ADCT (Az = 0.77, $p < 0.05$) and MR imaging with ultra-short TE (Az = 0.77, $p < 0.05$).

The diagnostic capability of each radiological index for differentiating nodules requiring aggressive intervention and treatment from nodules needing only follow-up examination is shown in Table 4. When applied each feasible threshold value, accuracy of total perfusion on dynamic first-pass CE-perfusion ADCT (90.1% [64/71]) and MR imaging with ultra-short TE (88.7% [63/71]) was significantly higher than that of systemic arterial perfusion for the two methods (80.3% [57/71], $p < 0.05$) and SUV_{max} (78.9% [56/71], $p < 0.05$).

4. Discussion

Our results demonstrate that quantitatively assessed first-pass component assessments based on dynamic first-pass CE-perfusion ADCT and MR imaging with ultra-short TE were more effective than those based on FDG-PET/CT for differentiation of malignant from benign nodules and distinguishing nodules requiring aggressive intervention and treatment from those needing only follow-up examination. In addition, since quantitatively assessed dynamic first-pass CE-perfusion ADCT and MR imaging with ultra-short TE had statistically similar potential, they could therefore be considered to have the potential to serve as substitutes for each other in this setting.

As for assessments of intra- and inter-observer agreements for each index, correlations between first and second measurements and between the two investigators were strong. In addition, the reproducibility coefficients and the limits of agreement for the indices used in our study were compatible with those published previously [3,9,12–15,17,18,20]. Moreover, evaluations of inter-method agreements for each of the perfusion index assessments showed significant and excellent correlations for dynamic first-pass CE-perfusion ADCT and MR imaging with ultra-short TE. Although the limits of agreement between the two investigators for each of the indices were relatively small, they were slightly larger than those for each modality. Moreover, all mean differences were less than 0 ml/100 ml/min. Our findings as well as those of previous studies indicate that evaluations using any of the radiological indices for dynamic first-pass CE-perfusion ADCT, dynamic first-pass CE-MRI with ultra-short TE and FDG-PET/CT are reproducible, and can therefore be used as objective measurements in routine clinical practice [3,9,12–15,17,18,20]. In addition, each perfusion index used with dynamic first-pass CE-perfusion MR imaging with ultra-short TE was somewhat overestimated when compared with that used with dynamic first-pass CE-perfusion ADCT.

Our results further demonstrate that dynamic first-pass CE-perfusion ADCT and MR indices derived from both the maximum slope method as well as SUV_{max} showed significant differences between malignant and benign nodules with predicted low biological activity as well as between nodules requiring further intervention and treatment and those needing no further evaluation. On the other hand, dynamic first-pass CE-perfusion ADCT and MR indices showed no significant differences between malignant and benign nodules with predicted high biological activity. Previously reported pharmacokinetic analyses of dynamic first-pass CT as well as dynamic MR imaging with ultra-short echo time (TE) indicated that the wash-in phase during the first transit of contrast media correlates with perfusion, microvascular density due to tumor angiogenesis, increased extracellular space for accumulation of contrast material, and permeability of capillaries [3,9,12–15,17,18,21–28]. Therefore, some overlap of dynamic first-pass CE-perfusion ADCT and CE-MR indices for malignant nodules and benign nodules with predicted high biological activity are to be expected in view of the underlying angiogenesis of malignant neoplasms and benign nodules with predicted high biological activity. When the pharmacokinetic background is taken into consideration, our findings are therefore compatible with those previously reported [3,9,12–15,17,18,21–28], and indicate that dynamic first-pass CE-perfusion ADCT indices obtained with the two maximum slope methods would be as effective as dynamic first-pass CE-MRI with ultra-short TE and PET/CT for assessment of SPN features.

The results of ROC analyses and comparisons of diagnostic performance for differentiation of malignant from benign nodules clearly showed that the total perfusion from dynamic first-pass CE-perfusion ADCT and MR imaging with ultra-short TE showed significantly larger Az values and higher accuracies than that from systemic arterial perfusion assessed by the two methods. In addition, accuracy of total perfusion obtained with either method was also significantly higher than that of SUV_{max}. This conclusion is partly compatible with that of previous reports [3,9,15–17]. Moreover, quantitatively assessed dynamic first-pass CE-ADCT and MR imaging with ultra-short TE showed similar potential, and should therefore be used to evaluated total perfusion rather than other indices in this setting. This finding and conclusion are first reported here.

When considering nodule management and the underlying pathologic and pharmacokinetic aspects of malignant as well as of benign nodules with high and low biological activities, it would be more advisable for clinicians to divide all nodules into two groups: nodules requiring aggressive intervention and treatment from those needing only follow-up examination. To this end, our results indicate that dynamic first-pass CE-perfusion ADCT and MR imaging with ultra-short TE should be used rather than PET/CT in this setting. Moreover, total perfusions obtained with the two methods yielded higher accuracy than that did either systemic arterial perfusions or SUV_{max}, a finding partly compatible with that previously reported [15,17]. Therefore, dynamic first-pass CE-perfusion ADCT and MR imaging with ultra-short TE have similar potential in this setting. Moreover, it would be advisable for clinicians to employ quantitatively assessed dynamic first-pass CE-perfusion ADCT or MR imaging with ultra-short TE rather than FDG-PET/CT for management of SPNs, provided any of these methods can be used appropriately in routine clinical practice at a given institution.

Our study has certain limitations. The mean nodule size of each group was less than 18 mm, which is larger than that of indeterminate nodules subjected to CT examination in routine clinical practice. The Fleishner Society currently recommends solid nodules, which don't have calcification and are more than 8 mm in diameter, to be subjected to further radiological and interventional examinations [29–31]. Therefore, distribution of nodule size, frequency of nodule calcification and prevalence of malignancy, as well as histological type of the benign nodules used in our study are likely to be different from those of nodules detected in routine clinical practice, and might therefore be a source of the bias in our study. Second, we used dynamic first-pass CE-perfusion ADCT and MR imaging with ultra-short TE on a 3 T MR system. In addition, we used commercially available perfusion software for dynamic first-pass CE-perfusion ADCT and our proprietary software for dynamic first-pass CE-perfusion MR imaging with ultra-short TE, but we did not assess other software provided by other vendors as well as used by other academic institutions. In addition, the numbers of SPNs

and subjects were limited in this study. Moreover, diffusion-weighted MR imaging, which is suggested as useful for assessment of pulmonary nodule [32], was not compared diagnostic performance with dynamic first-pass CE-perfusion ADCT and MR imaging as well as PET/CT. Therefore, large-scale prospective studies using other CT and MR systems as well as software with different mathematical models are warranted.

In conclusion, dynamic first-pass CE-perfusion MR imaging with ultra-short TE and ADCT have similar potential capabilities and are superior to FDG-PET/CT for differentiation of malignant from benign nodules. In addition, the same results were obtained for distinguishing nodules requiring aggressive intervention and treatment from those needing only follow-up examinations in routine clinical practice.

Conflict of interest

Three of the authors (Ms. Yasuko Fujisawa, Mr. Masao Yui and Mr. Naoki Sugihara) are employees of Canon Medical Systems Corporation, but did not have control over any of the data and information submitted for publication or which data and information were to be included in this study.

Acknowledgements

This work was supported by Grants-in-Aid for Scientific Research from the Japanese Ministry of Education, Culture, Sports, Science and Technology (JSTS.KAKEN; No. 24591762), the Adaptive and Seamless Technology Transfer Program through Target Driven R & D from the Japan Science and Technology (JST) Agency (AS2511335P), Canon Medical Systems Corporation, Bayer Pharma and Guerbet Japan.

Three of the authors (Yasuko Fujisawa, Masao Yui and Naoki Sugihara) are employees of Canon Medical Systems, Corporation, but did not have control over any of the data and information submitted for publication or which data and information were to be included in this study.

Appendix A. Supplementary data

Supplementary data associated with this article can be found, in the online version, at https://doi.org/10.1016/j.ejrad.2019.03.018.

References

[1] S.J. Swensen, R.W. Viggiano, D.E. Midthun, et al., Lung nodule enhancement at CT: multicenter study, Radiology 214 (1) (2000) 73–80.
[2] A. Matthies, M. Hickeson, A. Cuchiara, A. Alavi, Dual time point 18F-FDG PET for the evaluation of pulmonary nodules, J. Nucl. Med. 43 (7) (2002) 871–875.
[3] Y. Ohno, H. Hatabu, D. Takenaka, S. Adachi, M. Kono, K. Sugimura, Solitary pulmonary nodules: potential role of dynamic MR imaging in management: initial experience, Radiology 224 (2) (2002) 503–511.
[4] J.F. Schaefer, J. Vollmar, F. Schick, et al., Solitary pulmonary nodules: dynamic contrast-enhanced MR imaging-perfusion differences in malignant and benign lesions, Radiology 232 (2) (2004) 544–553.
[5] Y.J. Jeong, K.S. Lee, S.Y. Jeong, Solitary pulmonary nodule: characterization with combined wash-in and wash-out features at dynamic multi-detector row CT, Radiology 237 (2) (2005) 675–683.
[6] C.A. Yi, K.S. Lee, B.T. Kim, et al., Tissue characterization of solitary pulmonary nodule: comparative study between helical dynamic CT and integrated PET/CT, J. Nucl. Med. 47 (3) (2006) 443–450.
[7] S.L. Aquino, L.B. Kuester, V.V. Muse, E.F. Halpern, A.J. Fischman, Accuracy of transmission CT and FDG-PET in the detection of small pulmonary nodules with integrated PET/CT, Eur. J. Nucl. Med. Mol. Imaging 33 (6) (2006) 692–696.
[8] P. Cronin, B.A. Dwamena, A.M. Kelly, R.C. Carlos, Solitary pulmonary nodules: meta-analytic comparison of cross-sectional imaging modalities for diagnosis of malignancy, Radiology 246 (3) (2008) 772–782.
[9] Y. Ohno, H. Koyama, D. Takenaka, et al., Dynamic MRI, dynamic multidetector-row computed tomography (MDCT), and coregistered 2-[fluorine-18]-fluoro-2-deoxy-D-glucose-positron emission tomography (FDG-PET)/CT: comparative study of capability for management of pulmonary nodules, J. Magn. Reson. Imaging 27 (6) (2008) 1284–1295.
[10] I. Sitartchouk, H.C. Roberts, A.M. Pereira, H. Bayanati, T. Waddell, T.P. Roberts, Computed tomography perfusion using first pass methods for lung nodule characterization, Invest. Radiol. 43 (6) (2008) 349–358.
[11] Y. Li, Z.G. Yang, T.W. Chen, J.Q. Yu, J.Y. Sun, H.J. Chen, First-pass perfusion imaging of solitary pulmonary nodules with 64-detector row CT: comparison of perfusion parameters of malignant and benign lesions, Br. J. Radiol. 83 (993) (2010) 785–790.
[12] Y. Ohno, H. Koyama, K. Matsumoto, et al., Differentiation of malignant and benign pulmonary nodules with quantitative first-pass 320-detector row perfusion CT versus FDG PET/CT, Radiology 258 (2) (2011) 599–609.
[13] Y. Ohno, H. Koyama, Y. Fujisawa, et al., Dynamic contrast-enhanced perfusion area detector CT for non-small cell lung cancer patients: influence of mathematical models on early prediction capabilities for treatment response and recurrence after chemoradiotherapy, Eur. J. Radiol. 85 (1) (2016) 176–186.
[14] Y. Ohno, Y. Fujisawa, H. Koyama, et al., Dynamic contrast-enhanced perfusion area-detector CT assessed with various mathematical models: its capability for therapeutic outcome prediction for non-small cell lung cancer patients with chemoradiotherapy as compared with that of FDG-PET/CT, Eur. J. Radiol. 86 (2017) 83–91.
[15] Y. Ohno, M. Nishio, H. Koyama, et al., Comparison of quantitatively analyzed dynamic area-detector CT using various mathematic methods with FDG PET/CT in management of solitary pulmonary nodules, Am. J. Roentgenol. 200 (6) (2013) W593–W602.
[16] X. Yuan, J. Zhang, C. Quan, et al., Differentiation of malignant and benign pulmonary nodules with first-pass dual-input perfusion CT, Eur. Radiol. 23 (9) (2013) 2469–2474.
[17] Y. Ohno, M. Nishio, H. Koyama, et al., Solitary pulmonary nodules: comparison of dynamic first-pass contrast-enhanced perfusion area-detector CT, dynamic first-pass contrast-enhanced MR imaging, and FDG PET/CT, Radiology 274 (2) (2015) 563–575.
[18] Y. Ohno, H. Koyama, Y. Fujisawa, et al., Hybrid Type iterative reconstruction method vs. filter back projection method: capability for radiation dose reduction and perfusion assessment on dynamic first-pass contrast-enhanced perfusion chest area-detector CT, Eur. J. Radiol. 85 (1) (2016) 164–175.
[19] J. Piper, Y. Ikeda, Y. Fujisawa, et al., Objective evaluation of the correction by non-rigid registration of abdominal organ motion in low-dose 4D dynamic contrast-enhanced CT, Phys. Med. Biol. 57 (6) (2012) 1701–1715.
[20] J.M. Bland, D.G. Altman, Statistical methods for assessing agreement between two methods of clinical measurement, Lancet 1 (8476) (1986) 307–310.
[21] J.T. Littleton, M.L. Durizch, G. Moeller, D.E. Herbert, Pulmonary masses: contrast enhancement, Radiology 177 (3) (1990) 861–871.
[22] Robins, Acute and chronic inflammation, in: R.S. Cotran, V. Kumar, T. Collins (Eds.), Pathologic basis of disease, 6th ed., W.B. Saunders, Philadelphia, PA, 1999, pp. 50–88.
[23] E.N. Milne, Circulation of primary and metastatic pulmonary neoplasms. A post-mortem microarteriographic study, Am. J. Roentgenol. Radium Ther. Nucl. Med. 100 (3) (1967) 603–619.
[24] M. Oikawa, E.N. Milne, E. Whitmore, D. Gilday, C. Oliver, A morphological and quantitative study of tumor blood flow. I. During growth and immune rejection, Cancer 35 (2) (1975) 385–398.
[25] E.N. Milne, Pulmonary metastases: vascular supply and diagnosis, Int. J. Radiat. Oncol. Biol. Phys. 1 (7–8) (1976) 739–742.
[26] E.N. Milne, Pulmonary blood flow distribution, Invest. Radiol. 12 (6) (1977) 479–481.
[27] E.N. Milne, E.A. Zerhouni, Blood supply of pulmonary metastases, J. Thorac. Imaging 2 (4) (1987) 15–23.
[28] Y. Ohno, M. Nishio, H. Koyama, et al., Dynamic contrast-enhanced CT and MRI for pulmonary nodule assessment, Am. J. Roentgenol. 202 (3) (2014) 515–529.
[29] H. MacMahon, J.H. Austin, G. Gamsu, et al., Fleischner Society. Guidelines for management of small pulmonary nodules detected on CT scans: a statement from the Fleischner Society, Radiology 237 (2) (2005) 395–400.
[30] D.P. Naidich, A.A. Bankier, H. MacMahon, et al., Recommendations for the management of subsolid pulmonary nodules detected at CT: a statement from the Fleischner Society, Radiology 266 (1) (2013) 304–317.
[31] H. MacMahon, D.P. Naidich, J.M. Goo, K.S. Lee, A.N.C. Leung, J.R. Mayo, A.C. Mehta, Y. Ohno, C.A. Powell, M. Prokop, G.D. Rubin, C.M. Schaefer-Prokop, W.D. Travis, P.E. Van Schil, A.A. Bankier, Guidelines for management of incidental pulmonary nodules detected on CT images: from the Fleischner Society 2017, Radiology 284 (1) (2017) 228–243.
[32] A. Basso Dias, M. Zanon, S. Altmayer, G. Sartori Pacini, N. Henz Concatto, G. Watte, A. Garcez, T.L. Mohammed, N. Verma, T. Medeiros, E. Marchiori, K. Irion, B. Hochhegger, Fluorine 18-FDG PET/CT and diffusion-weighted MRI for malignant versus benign pulmonary lesions: a meta-analysis, Radiology (2018) Nov. 27: 181159, doi: 10.1148/radiol.2018181159. [Epub ahead of print].